MAJOR METABOLITES FROM *HYPERICUM PERFORATUM* L., HYPERFORIN AND HYPERICIN, ARE BOTH ACTIVE AGAINST HUMAN CORONAVIRUSES

Raczkiewicz I.[1], Rivière C.[2]*, Bouquet P.[1]*, Desmarets L.[1], Tarricone A.[1], Camuzet C. [1], François N.[1], Lefèvre G.[2], Samaillie J.[2], Silva Angulo F.[1], Robil C. [1], Trottein F.[1], Sahpaz S.[2], Dubuisson J.[1], Belouzard S. [1], Goffard A.[1], Séron K.[1]†

[1] Univ. Lille, CNRS, Inserm, CHU Lille, Institut Pasteur de Lille, U1019 – UMR9017 – Center for Infection and Immunity of Lille (CIIL), F-59000 Lille, France

[2] BioEcoAgro, Joint Research Unit 1158, Univ. Lille, INRAE, Univ. Liège, UPJV, YNCREA, Univ. Artois, Univ. Littoral Côte d'Opale, ICV – Institut Charles Viollette, F-59650 Villeneuve d'Ascq, France

†corresponding author

E-mail: karin.seron@ibl.cnrs.fr

* These authors contributed equally to this work

ABSTRACT

COVID-19 pandemic has highlighted the need of antiviral molecules against coronaviruses. Plants are an endless source of active compounds. In the current study, we investigated the potential antiviral effects of *Hypericum perforatum* L.. Its extract contained two major metabolites belonging to distinct chemical classes, hypericin (HC) and hyperforin (HF). First, we demonstrated that HC inhibited HCoV-229E at the entry step by directly targeting the viral particle in a light-dependent manner. While antiviral properties have already been described for HC, the study here showed for the first time that HF has pan-coronavirus antiviral capacity. Indeed, HF was highly active against Alphacoronavirus HCoV-229E (IC_{50} value of 1.10 µM), and Betacoronaviruses SARS-CoV-2 (IC_{50} value of of 0.24 to 0.98 µM), SARS-CoV (IC_{50} value of 1.01 µM) and MERS-CoV (IC_{50} value of 2.55 µM). Unlike HC, HF was active at a post-entry step, most likely the replication step. Antiviral activity of HF on HCoV-229E and SARS-CoV-2 was confirmed in primary human respiratory epithelial cells. Furthermore, *in vitro* combination assay of HF with remdesivir showed that their association was additive, which was encouraging for a potential therapeutical association. As HF was active on both Alpha- and Betacoronaviruses, a cellular target was hypothesized. Heme oxygenase 1 (HO-1) pathway, a potential target of HF, has been investigated but the results showed that HF antiviral activity against HCoV-229E was not dependent on HO-1. Collectively, HF is a promising antiviral candidate in view of our results and pharmacokinetics studies already published in animal models or in human.

41 **INTRODUCTION**

42 The recent COVID-19 pandemic caused by severe acute respiratory syndrome
43 coronavirus 2 (SARS-CoV-2) has highlighted the urge for broad-spectrum antivirals. Before the
44 emergence of SARS-CoV-2, no specific coronavirus (CoV) antiviral agent was available. Four
45 years after the beginning of the outbreak, we are still lacking for therapeutical options. To
46 date, there are only three direct-acting antivirals (DAA) approved by FDA (Food and Drug
47 Administration) for clinical usage. The ritonavir-boosted nirmatrelvir (Paxlovid®) is the first
48 line-therapy for patients with high risk of developing severe COVID-19. Nirmatrelvir (PF-
49 07321332) is an oral protease inhibitor that is active against the main protease (M^{PRO}) of SARS-
50 CoV-2 (1). Ritonavir serves as a booster, since it increases the plasma concentration of
51 nirmatrelvir by inhibiting the cytochrome P450 3A4 (2). The second-line therapy, remdesivir is
52 often given when there is contraindication to Paxlovid®. Remdesivir (GS-5734), a viral RNA-
53 dependent RNA polymerase (RdRp) inhibitor initially developed to treat Ebola infections, was
54 one of the first molecule to demonstrate an antiviral activity against CoV *in vitro* and *in vivo*
55 (3–5). Given intravenously, remdesivir which is an adenosine nucleotide analog prodrug, acts
56 as a chain-terminator (6). The third-line therapy, molnupiravir (MK-4482 or EIDD-2801), a
57 RdRp inhibitor originally developed against hepatitis C virus (HCV) infection, is an orally
58 available prodrug of the ribonucleoside analog EIDD-1931 (β-D-N4-hydroxycytidine) that has
59 a broad-spectrum antiviral activity against RNA viruses (7, 8). Even though these therapies are
60 widely used, some concerns remain. Firstly, even if they are still active against the current
61 circulating variants, the increased use of antivirals supports the development of drug
62 resistance (9, 10). One of the main strategies to avoid the emergence of resistant mutants is
63 the use of combination therapies that allow complete viral clearance, especially in
64 immunocompromised patient (11–13). Secondly, 2% of Paxlovid® treated patients have
65 exhibited a viral rebound, which is not significantly different from the placebo group (14, 15).
66 Thirdly, the poor bioavailability of remdesivir when taken orally makes it challenging for
67 ambulatory care and limits its usage for hospital settings. Fourthly, although molnupiravir is
68 still approved by FDA, it has been withdrawn by the European Medicines Agency (EMA)
69 because the benefice-risk balance was unfavorable for the patient (16). Finally, molnupiravir
70 could pose a risk to the host, as it has been shown to have mutagenic potential in human cells
71 (17). In light of these challenges, the development of new antivirals is more than necessary.

72 CoVs are positive single stranded-RNA viruses belonging to the *Coronaviridae* family,
73 the *Orthocoronavirinae* subfamily and the Nidovirales order (18). Seven CoV infect human
74 (HCoV) so far and can be distinguished into two groups based on the clinical presentation,
75 from mild, HCoV-229E, -OC43, -HKU1, and -NL63, to severe symptoms, SARS-CoV, Middle-East
76 respiratory syndrome coronavirus (MERS-CoV) and SARS-CoV-2 (19). Coronaviruses are
77 enveloped RNA viruses. Structural proteins spike (S), envelope (E), and membrane (M)
78 proteins are embedded into the envelope lipid bilayer and protect the viral genome which is
79 associated with nucleoprotein (N). The S protein mediates the host-cell attachment and the
80 viral entry by recognizing host-specific receptors (20). The virus enters into the cell via two
81 different pathways, depending on the expression of cellular proteases on the cell surface, such
82 as TMPRSS2 (21). If the latter is expressed, the S protein is cleaved at the cell surface and the
83 viral particle fuses with host plasma membrane. The endosomal pathway is the second entry
84 pathway and the fusion occurs with the endosomal membrane (22). The genome is then
85 released into the cytosol, where it is translated into two polyproteins, pp1a and pp1ab. These
86 two are cleaved by the papain-like protease nsp3 (PL^{pro}) and the main protease nsp5 (M^{PRO}),
87 into several nonstructural proteins (nsp) such as nsp12, the viral RdRp, engaging the
88 replication step (23). Then the virus is assembled and secreted.
89 According to World Health Organization, around 80% of the population relies on herbal
90 medicine to heal themselves, and plants are a great source of active molecules with huge
91 structural diversity. Several natural products have been shown to exhibit antiviral activity
92 against viruses of different families *in vitro* (24). We have recently shown that pheophorbide a
93 (Pba), a chlorophyll degradation product is active against SARS-CoV-2 and MERS-CoV (25), that
94 the red algae derivate griffithsin is active against MERS-CoV (26), and that some cinnamoyl
95 oleanolic acids isolated from *Hippophae rhmnoides* are active against both SARS-CoV-2 and
96 HCoV-229E (27). Also, we believe that plants could contain promising antiviral molecules of
97 different chemical classes that are still unknown.
98 *Hypericum* Tourn ex L. is a cosmopolitan genus with 512 recognized species to date
99 (28). *Hypericum perforatum* L. (perforated Saint John's wort, SJW), belonging to Hypericaceae,
100 is the most common and well-known species among this genus (29). Its chemical composition
101 includes flavonols (quercetin and its glycosides including hyperoside, rutin, isoquercitrin,
102 quercitrin, miquelianin), biflavonoids (I3,II8-biapigenin and amentoflavone),
103 naphtodianthrones (hypericin (HC) and its analogues), prenylated phloroglucinols (hyperforin

104 (HF) and its analogues) (30). Some standardized extracts of SJW, have been studied in many
105 clinical trials to assess their effectiveness in depression also demonstrating a good tolerability
106 (31–33). However, HC appears to induce adverse effects such as phototoxicity (34) and HF is
107 known to be an enzyme inducer (31). HF and HC are the active compounds of *Hypericum*
108 *perforatum* L. known to be responsible for its anti-depressive properties. To date, only HC has
109 been described for antiviral activity against enveloped viruses such as human
110 immunodeficiency virus 1, Sindbis virus and murine cytomegalovirus with a light-dependent
111 activity (35). More recently, an antiviral activity against SARS-CoV-2 has been discovered for
112 this naphtodianthrone (36).

113 Here we highlighted that two major metabolites of *Hypericum perforatum* L., HC and
114 HF, exhibit antiviral activity against HCoV, with distinct modes of action with HC inhibiting
115 entry of HCoV an HF a post-entry step. Furthermore, our data described for the first time an
116 antiviral capacity for HF with pan-coronavirus activity.

117

118

119 **RESULTS**

120 ***1. Hypericum perforatum* L. *and its metabolites, HF and HC, are active against HCoV-***
121 ***229E***

122 In order to identify new antiviral compounds against HCoVs, we have selected the crude
123 methanolic extract of *Hypericum perforatum* L. based on a previous screening of several
124 plants. Its antiviral activity was tested against HCoV-229E-Luc in a dose-response assay. The
125 results showed that the crude methanolic extract inhibited HCoV-229-Luc infection in a dose-
126 dependent manner with 50% inhibitory concentration (IC_{50}) of 18.73 ± 0.84 µg/mL (**Figure 1A**).
127 No cytotoxicity was observed at active concentrations (**Figure 1A**). The results suggested the
128 presence of at least one active compound within *Hypericum perforatum* L. crude extract which
129 is known to contain two major metabolites, HF, a prenylated phloroglucinol derivative, and
130 HC, an anthraquinone derivative. To determine if these compounds were responsible for the
131 anti-coronavirus activity, dose-response and cytotoxicity assays were performed. The results
132 showed that the two metabolites exhibited antiviral activity against HCoV-229-Luc with IC_{50}
133 values of 0.37 ± 0.02 µM and 1.10 µM ± 0.08 µM, respectively (**Figures 1B and C**). Cytotoxicity
134 tests showed that both compounds are not toxic at active concentrations with a 50% cytotoxic

135 concentration (CC_{50}) values of 25.77 ± 2.58 µM and 19.35 ± 2.08 µM for HC and HF,
136 respectively, resulting in a selective index (SI) of 69 for HC and 17 for HF (**Figures 1B and C**).
137
138 ***2. HC inhibits the entry of HCoV-229E in a light-dependent manner and by directly***
139 ***targeting the viral particle***
140 We further investigated each active compound individually to determine their mechanism of
141 action. It was recently underlined that HC inhibited SARS-CoV-2 at the entry step (36). To
142 characterize the mechanism of action of HC on HCoV-229E, a time-of-addition assay was
143 performed by adding the compound at 4 µM (corresponding to the IC_{90}) at different
144 timepoints during infection, either before, during or after the inoculation of the cells by the
145 virus (**Figure 2A**). The results showed that HC significantly reduced HCoV-229E-Luc infection
146 when added from pre-treatment condition to 2 h post-inoculation (p.i.), meaning that it
147 inhibited the infection at an early step (**Figure 2B**), probably the entry step. An entry assay
148 was performed with particles pseudotyped with HCoV-229E S protein (229pp) and mimicking
149 virus entry, in the presence of HC. The results showed that HC significantly decreased 229Epp
150 entry in a dose-dependent manner (**Figure 2C**). Taken together, these results highlighted that
151 HC is an inhibitor of HCoV-229E entry, which is consistent with already published data on
152 SARS-CoV-2.
153 To inhibit viral entry, a compound may act directly on the viral particle before its attachment
154 to the cell surface. To assess if HC was such inhibitor, we incubated HCoV-229E-Luc with HC at
155 high concentration (2 µM) for 30 min. Then, before inoculation, we diluted the mixture 10
156 times to reach a final concentration of HC of 0.2 µM. This concentration is inactive on HCoV-
157 229E. As controls, cells were inoculated by HCoV-229E-Luc in the presence of HC either at
158 "high" concentration (2 µM) and "low" concentration (0.2 µM). It is important to note that
159 the MOI was kept constant in all conditions. The results showed no significant inhibition of
160 infection in presence of 0.2 µM HC, whereas a similar significant inhibition of infection was
161 observed for the condition "2 µM > 0.2 µM" HC and infection with 2 µM HC (**Figure 2D**). Taken
162 together these results showed that HC targeted the viral particle before infection. It is well
163 known that HC is a photoactivable molecule and has a light-dependent activity on several
164 viruses (35). To determine if antiviral activity of HC on HCoV-229E is light-dependent, a dose-
165 response assay was carried out in the presence or absence of light. The white visible light is
166 sufficient to photoactivate HC, so we used the light of the safety cabinet (37). The results

167 confirmed the dose-dependent inhibition of infection of HCoV-229E-Luc in the presence of HC
168 under normal light condition (**Figure 2E**) similar to the results presented in **Figure 1B**.
169 However, when the experiment was carried out in the dark, no inhibition of HCoV-229E-Luc
170 infection was observed even at high HC concentration up to 5 µM (a concentration above IC_{90}
171 under light exposure) (**Figure 2E**). These results clearly demonstrated that HC directly targets
172 the viral particle and inhibits HCoV-229E entry in a light-dependent manner.
173

174 ***3. HF has a pan-coronavirus antiviral activity***

175 HF is less studied than HC in literature and no data are available on its potential antiviral
176 activity. Thus, we performed antiviral assays against three highly pathogenic HCoVs, SARS-
177 CoV, MERS-CoV and SARS-CoV-2. For SARS-CoV-2, we had access to different variants, the
178 initial Wuhan strain (D614), alpha variant B1.1.7 and omicron variant B1.1.529. Dose-response
179 inhibition studies were conducted and the results were shown in **Figure 3**. Antiviral assays on
180 SARS-CoV-2 variants were performed in Vero-81/TMPRSS2 cells and antiviral activity was
181 assessed by viral titration. The results showed that HF inhibited infection of all tested SARS-
182 CoV-2 variants with calculated IC_{50} values of 0.98 $\pm$ 0.28 µM, 0.24 $\pm$ 0.02 µM, and 0.29 $\pm$ 0.13
183 µM for strain D614, alpha variant B1.1.7 and omicron variant B1.1.529 respectively, without
184 any cytotoxicity at the active concentration (CC_{50} = 45.91 µM) (**Figure 3A**). The respective SI
185 were all higher than 40 (**Table 2**). These data were confirmed by Western blot analyses in
186 human lung A549/ACE2 cells infected with SARS-CoV-2 alpha variant (**Figure 3B**). A dose-
187 dependent decrease of the expression of SARS-CoV-2 N protein was observed in presence of
188 HF. Dose-response assays were also conducted against the two others highly pathogenic
189 HCoVs, SARS-CoV and MERS-CoV, in Vero-81/TMPRSS2 and Calu-3 cells, respectively. Our
190 results highlighted that HF is highly active against both SARS-CoV and MERS-CoV with an IC_{50}
191 values of 1.01 $\pm$ 0.12 µM and 2.55 $\pm$ 0.28 µM, respectively, resulting in SI of 45 for SARS-CoV
192 (**Figure 3C and 3D, Table 2**). CC_{50} value in Calu-3 cells was not determined precisely, but, as
193 observed in **Figure 3D**, it was higher than 20 µM, with SI>7. Taken together, these data
194 suggested that HF has a pan-coronavirus antiviral activity with IC_{50} values ranging from 0.24
195 to 2.55 µM.
196
197
198
199

200 **Table 1.** Cytotoxicity and antiviral activity of HF against HCoVs. ND: not determined.

Virus	Cells	IC_{50} (µM)	CC_{50} (µM)	SI
HCoV-229E	Huh-7/TMPRSS2	1.10 ± 0.08	19.35 ± 2.08	17
SARS-CoV-2 (D614)	Vero-81/TMPRSS2	0.98 ± 0.28	45.91 ± 4.85	46
SARS-CoV-2 alpha (B1.1.7)	Vero-81/TMPRSS2	0.24 ± 0.02	45.91 ± 4.85	188
SARS-CoV-2 omicron (B1.1.529)	Vero-81/TMPRSS2	0.29 ± 0.13	45.91 ± 4.85	158
SARS-CoV	Vero-81/TMPRSS2	1.01 ± 0.12	45.91 ± 4.85	45
MERS-CoV	Calu-3	2.55 ± 0.28	> 20.0	ND

201

202 ***4. HF is an inhibitor of HCoV replication step***

203 To characterize the mechanism of action of HF against HCoVs, time-of-addition assays against
204 HCoV-229E and SARS-CoV-2 were performed. The data presented in **Figure 4A** and **4B** showed
205 a higher inhibition of infection when HF was added at 1 h to 3 h p.i., for both HCoV-229E-Luc
206 and SARS-CoV-2. Although HF significatively inhibited the infection of HCoV-229E at all steps
207 (from pre-treatment to 3 h p.i.), it decreased the infection by more than $2xLog_{10}$ from 1 h p.i.
208 to 3 h p.i. (**Figure 4A**). Similar results were observed with SARS-CoV-2; N protein was not
209 detected when HF was added from 1 h to 3 h p.i. (**Figure 4B**). Pba, a natural compound
210 targeting the viral envelope, and GC376, a protease inhibitor, were added as an entry and a
211 replication inhibitor, respectively. Similar profiles of N expression were observed with GC376
212 and HF. Chloroquine was used to control the expression of TMPRSS2. These data suggested
213 that HF is an inhibitor of the replication step of both SARS-CoV-2 and HCoV-229E.
214 To confirm this hypothesis, entry inhibition assays were performed with either 229Epp and
215 SARS2pp. No significant decrease of infection was observed for any of the particles in the
216 presence of HF up to 5 µM (**Figure 4C**) confirming that HF is not an entry inhibitor. Altogether
217 these data suggested that HF is an inhibitor of HCoV post-entry step, most likely the replication
218 step.

219

220 ***5. HF inhibits HCoV-229E and SARS-CoV-2 infection in human primary epithelial cells***

221 To gain relevance, the antiviral activity of HF was then tested in human primary airway cells
222 cultivated at air-liquid interface, considered as a preclinical model for human coronaviruses.
223 First, the cytotoxicity of HF in human airway epithelia (MucilAir^{TM}-HAE) was determined by
224 measuring LDH secretion and TEER at 24 and 48 h. LDH secretion higher than 5 % and TEER
225 lower than 100 $\Omega.cm^2$ reflect damaged cells. No cytotoxicity was observed with 4 µM HF at 24

226 and 48 h for the two measured parameters (**Figures 5A and B**). However, cytotoxicity was
227 observed with 12 µM HF at 48 h, with LDH secretion higher than 5% compared to control and
228 TEER lower than 100 Ω.cm^2 (**Figures 5A and B**). Thus, for antiviral assays, two HF
229 concentrations, 4 and 12 µM, were tested against HCoV-229E-Luc and only one, 4 µM, against
230 SARS-CoV-2 due to a longer incubation time of 48 h.
231 HAE were inoculated with HCoV-229E-Luc in the presence of 4 or 12 µM HF and 10 µM GC376
232 as a control, for 24 h. Viral RNA at the apical surface was quantified as well as luciferase activity
233 in cell lysates. The results showed a decrease in viral RNA copies and luciferase activity when
234 cells were treated with 12 µM HF (**Figures 5C and D**), similar to the decrease observed with 10
235 µM GC376. These results highlighted that HF is active against HCoV-229E in human primary
236 cells.
237 To determine if HF could also inhibit SARS-CoV-2 in this preclinical model, HAE were inoculated
238 with the virus in the presence of 4 µM HF. Viral infectious titers at the apical surface and
239 intracellular viral RNA were quantified (**Figures 5E and F**). The data showed a decrease of both
240 viral RNA copies and infectious titers in the presence 4 µM HF. A 3xLog_{10} decrease in viral titers
241 was observed upon 4 µM HF treatment similar to the decrease observed with 5 µM remdesivir
242 demonstrating that HF is an inhibitor of SARS-CoV-2 infection in HAE.
243 Taken together, these data underlined that HF is active against HCoVs in human primary
244 respiratory epithelial cells grown in air-liquid interface.
245
246 ***6. HF has an additive effect with remdesivir***
247 The results presented in this study demonstrate that HF encompasses many characteristics of
248 an antiviral agent to be used in therapy. In order to determine the potential use of HF as
249 therapeutic in clinic, combination studies of HF with remdesivir and nirmatrelvir, were
250 performed. Checkboard assays were performed with double serial dilutions of HF and
251 remdesivir or nirmatrelvir (**Figure 6**).
252 F1G-Red Vero-81 reporter cell line was used to monitor SARS-CoV-2 infection (38). First, the
253 cytotoxicity of each combination was assessed by quantifying the number of nuclei. No
254 cytotoxicity was observed for any of the combinations of HF with remdesivir or nirmatrelvir
255 (**Supplemental Figure 1**). The combination effect was then assessed with SynergyFinderPlus.
256 As shown in **Figure 7C**, the combination of HF with remdesivir is additive, with synergy scores

257 ranging from -10 to +10, with the four mathematical models (HSA, Loewe, Bliss and ZIP) and
258 significant *p*-value (**Table 2**).

259 **Table 2. Synergy scoring obtained from Synergy Finder for HF and remdesivir combination**.

Model	Synergy score	*p*-value
ZIP	4.23	4.44e-04
Loewe	3.09	5.22e-03
HAS	7.05	5.42e-23
Bliss	5.13	9.11e-07

260 A synergistic area, score above 10, was highlighted with HF, ranging from 2.5 to 10 µM,
261 combined to remdesivir, ranging from 37.5 to 150 nM, with a synergy score of 14.9 (**Figure**
262 **7B**). For nirmatrelvir, none of the mathematical model was able to give a significant synergy
263 score (**Supplemental Table 2**).
264

265 ***7. The antiviral activity of HF is not dependent of HO-1 pathway.***

266 Due to the pan-coronavirus antiviral activity of HF, we put forward the hypothesis that it may
267 regulate a cellular factor necessary for HCoVs replication. Recently, HF was described as an
268 inducer of heme oxygenase 1 (HO-1) pathway by upregulating the expression of HO-1 (39).
269 Moreover, it was also recently shown that hemin, an HO-1 inducer that upregulates HO-1
270 expression, has an antiviral activity against SARS-CoV-2 (40). HO-1 pathway was also described
271 to be involved in antiviral immune response against different viruses (41). Thus, we
272 hypothesized that the antiviral activity of HF against HCoV could be linked to the HO-1
273 pathway. To evaluate this hypothesis, Huh-7 cells or Vero81 cells were treated with increasing
274 concentrations of HF and then HO-1 protein expression was detected by Western Blot. The
275 results showed that HF up to 10 µM (active antiviral concentration; 10 x IC_{50}) was not able to
276 upregulate HO-1, unlike hemin, used as a control, which induced a strong up regulation of the
277 protein expression (**Figure 8A)**. Next, to further confirm these results, siRNA targeting HO-1
278 (siHO-1) were used to knock-down its expression prior to infection of Huh-7 cells with HCoV-
279 229E. HO-1 protein expression was strongly decreased by siHO-1, and was weakly induced by
280 hemin (**Figure 8B**). However, similar HF antiviral activities against HCoV-229E were observed
281 in wild-type Huh-7 cells compared to siHO-1 cells (**Figure 8C**). Taken together, the results
282 highlighted that HO-1 pathway is not involved in HF antiviral activity against HCoV-229E.
283
284

285 **DISCUSSION**

286 The development of broad-spectrum antiviral agents has become a necessity to
287 support the pandemic preparedness. Natural compounds are a great source of active
288 compounds with biological activities, including among others anticancer, antibacterial or
289 antiviral properties (42). Although there are no natural antiviral molecules used in clinical
290 settings yet, some plant extracts are currently being tested in clinical trials, like Antiwei
291 granule (a mix of Chinese herbs) for the treatment of influenza (43), *Viola odora* L. against
292 SARS-CoV-2 infection (44) or *Sutherlandia frutescens* (L.) R.Br. against HIV infection (45).

293 Here, we showed that HF, a major metabolite of SJW (*Hypericum perforatum* L.), a
294 prenylated phloroglucinol, has antiviral capacity against highly pathogenic HCoVs, SARS-CoV,
295 MERS-CoV, and SARS-CoV-2, and the low pathogenic HCoV-229E. Moreover, HF was active in
296 combination with remdesivir and in human primary airway cells. In addition, we highlighted
297 that HF might be an inhibitor of the replication step. Interestingly, HC, the second major
298 metabolite of SJW, a naphtodianthrone, displayed also antiviral capacities against HCoV-229E
299 infection but with a different mechanism of action than HF.

300 We demonstrated that HC has photo-dependent activity and targeted the viral particle.
301 The light-dependent mechanism of action of HC is consistent with previous reports on other
302 enveloped viruses such as human immunodeficiency virus 1, Sindbis virus and murine
303 cytomegalovirus (35, 46). Nonetheless, its light-dependent mechanism of action and its
304 phototoxicity are not compatible with clinical application in infected patients (34), but can be
305 potentially of interest for an environment disinfectant. Consequently, we focused our study
306 on characterization of HF antiviral activity.

307 We demonstrated that HF displayed pan-coronavirus activity, a feature that makes this
308 natural compound quite unique in the literature. Without any structural modification, IC_{50}
309 values are close to 1 µM, HCoV-229E (IC_{50} = 1.10 µM), SARS-CoV-2 (IC_{50} = 0.24 – 0.98 µM),
310 SARS-CoV (IC_{50} = 1.01 µM) and MERS-CoV (IC_{50} = 2.5 µM). Pharmacokinetics and bioavailability
311 data are already available in the literature for SJW's extract. It is important to note that
312 hyperforin is the major metabolite and hypericin is less abundant (up to 4.5% and 0.15% of
313 the extract, respectively) (47). Indeed, different studies show that the circulating
314 concentration of HF is within the range of our IC_{50} values with a maximal concentration of
315 690 nM and 1100 nM in rats and mice models, respectively, after administration of 300 mg/kg
316 of SJW extract and 5.2 mg/kg of hyperforin, respectively (48, 49). In human, ingestion of a

317 single dose of 300 – 1200 mg SJW's extract (containing 5 % of HF) led to a detectable
318 concentration of hyperforin in plasma ranging between 200 and 300 nM in healthy volunteers
319 in two different studies (48–50). Moreover, different reports also demonstrated that St John's
320 Wort extract was neither toxic in animal models nor in humans (31, 47, 51).

321 Although these results are encouraging, the distribution of HF in lungs after oral
322 administration has not been reported yet. Donà *et al.* (52) showed that HF was able to reduce
323 lung metastases in mice after intraperitoneal injection, demonstrating that the compound was
324 able to reach lungs *in vivo*. Our results in HAE demonstrated that HF is active when
325 administrated at the air interface. It would be interesting to quantify HF in the lungs after
326 intranasal administration. Pharmacokinetics studies are needed to optimize the dose and the
327 route of administration. Moreover, HF or SJW formulation might also be optimized to increase
328 their bioavailability (49, 50).

329 Besides the two major metabolites, HF and HC, the crude extract of *Hypericum*
330 *perforatum* L. also exhibited antiviral activity against HCoV-229E and SARS-CoV-2 (our data
331 and (36)). *Hypericum perforatum* L. is one out of more than 500 species of *Hypericum*
332 described so far. The composition in these two metabolites is very variable within these
333 species. It would be very interesting to correlate the antiviral activity of *Hypericum* species
334 with their composition. This will help to determine if the antiviral activity is mainly driven by
335 HF or HC, or if both may have additive or synergistic effect. We showed that HF and HC had
336 different mechanism of action, entry inhibition for HC and translation or replication inhibition
337 for HF. Consequently, it could be expected that these two compounds may have, at least, an
338 additive antiviral effect.

339 To avoid resistance, it is admitted that antiviral therapy should combine 2 or 3 antiviral
340 agents. Our results showed that HF could be associated with remdesivir, a RdRp inhibitor, with
341 additive antiviral activity, and synergistic at high concentration, *in vitro*. This result is
342 promising, but, unfortunately, no combination of HF with nirmatrelvir, the anti-protease agent
343 of Paxlovid, lacked additive or synergistic effect. However, no antagonist effect was observed,
344 showing that HF could still be envisaged as a promising antiviral agent. More experiments are
345 needed to explain these results.

346 Here we demonstrated that HF is active against all the highly pathogenic HCoVs
347 described so far, SARS-CoV, MERS-CoV and SARS-CoV-2. They all belong to the
348 Betacoronavirus genus. Interestingly, HF was also active against HCoV-229E which is a

349 member of the Alphacoronavirus genus. It would be interesting to test the antiviral capacity
350 of HF against other human and animal CoVs. HF time-of-addition assay on HCoV-229E and
351 SARS-CoV-2 suggested that HF could inhibit the replication step. Indeed, HF has a similar
352 kinetic profile as GC-376, a SARS-CoV-2 Mpro inhibitor. We thus hypothesized that HF might
353 target a cellular factor necessary for coronavirus replication, because it seemed unlikely that
354 HF could target a viral protein with similar efficacy for Alpha- and Betacoronavirus. A possible
355 cellular target, HO-1, was identified. A recent study has shown that HO-1 pathway is activated
356 upon treatment of melanoma cells with HF (39). Moreover, agonists of HO-1 pathway, such
357 as hemin, are known to exhibit antiviral activity against SARS-CoV-2 (40). However, our results
358 suggested that the antiviral activity of HF is not linked to HO-1 pathway. First, upregulation of
359 HO-1 protein expression was not observed neither in Huh-7 cells nor in Vero81 cells upon HF
360 treatment. It was shown by others that HO-1 expression could be induced in these cell types
361 when treated with agonists such as hemin (40, 53–56). Second, the knock-down of HO-1
362 expression in Huh-7 cells did not impair HCoV-229E infection. Further investigations are
363 needed to fully characterize the HF mechanism of action. Transcriptomic and proteomic
364 analyses may help to identify cellular genes or proteins whose expression is regulated by HF.
365 In conclusion, SJW extract and HF might be of great interest for future therapies on
366 HCoV or animal coronaviruses. A proof of their efficacy *in vivo* is still needed. However, efficacy
367 of HF against 4 different HCoVs makes this molecule particularly interesting in a pandemic
368 preparedness approach, in the event of the emergence of a new highly pathogenic HCoV.
369 Lately, new SARS-Like CoVs have been described in bats and are still a threat for human health
370 (57, 58).
371
372
373 **MATERIALS AND METHODS**
374 **Chemicals**
375 Dulbecco's modified Eagle's medium (DMEM), phosphate-buffered saline (PBS), 4',6-
376 diamidino-2-phenylindole (DAPI), GlutaMAX™ and Lipofectamine RNAi MAX were purchased
377 from Life Technologies (Carlsbad, California, USA). Goat and fetal bovine sera (FBS) were
378 obtained from Eurobio (Evry, France). Mowiol 4-88 was obtained from Calbiochem
379 (Darmstadt, Germany). Remdesivir (GS-5734) and tariquidar were from BioTechne
380 (Minneapolis, USA). Nirmatrelvir was from MedChemExpress (Monmouth Junction, USA). GC-

381 376 was obtained from AmBeed (Arlington Heights, USA). Chloroquine was from Sigma-
382 Aldrich (Saint Louis, USA). HC and HF were purchased from Phytolab (Vestenbergsgreuth,
383 Germany) (total of HF > 98.0%). Pba was from Cayman Chemicals (Merck Chemicals,
384 Darmstadt, Germany). Stocks of compounds were resuspended in dimethyl sulfoxide (DMSO)
385 at 100 mM. Plant extracts were resuspended in DMSO at 50 mg/ml.
386
387 **Antibodies**
388 Polyclonal rabbit anti-SARS-CoV-2 nucleocapsid antibody was purchased from Novus
389 Biological (Cambridge, UK). Mouse anti-dsRNA mAb (clone J2) was from Scicons (Nordic-
390 MUbio, Susteren, the Netherlands). Rabbit polyclonal anti-MERS-CoV Spike protein antibody
391 was from SinoBiological (Eschborn, Germany). Mouse anti-ß-tubulin IgG1 antibody (T5201)
392 was from Sigma. Monoclonal rabbit anti-HO-1 antibody was purchased from Cell Signaling
393 Technology (Danvers, Massachusetts). Horseradish peroxidase-conjugated goat anti-rabbit
394 IgG antibody, goat anti-mouse IgG antibody, Alexa 594-conjugated goat anti-rabbit antibody
395 and Alexa 488-conjugated donkey anti-mouse antibody, were purchased from Jackson
396 ImmunoResearch (Ely, United Kingdom).
397
398 **Cells**
399 Human kidney cell lines (HEK293T/17, ATCC, CRL-11268; HEK293TT/ACE2) (59), African green
400 monkey kidney cell lines (Vero-81, ATCC, CCL-81; Vero-E6 cells), Human lung cell line
401 (A549/ACE2, kindly provided by Delphine Muriaux), and Human hepatoma cells (Huh-7) were
402 grown in DMEM supplemented with 10% FBS.
403 Human lung cell line Calu-3 (ATCC, HTB-55) was cultivated in MEM supplemented with 10%
404 FBS and glutaMAX-1.
405 Lentiviral vectors expressing TMPRSS2 were used to transduce Vero-81 cells and to produce
406 Huh-7/TMPRSS2 stable cell line. This latter was selected with 2 µg/mL of puromycin. A
407 reporter cell line, F1G-Red, generated in the laboratory, and derivates from Vero-81 cells was
408 also used for combination assay (38). Primary human nasal epithelia MucilAir^{TM} (Epithelix,
409 Geneva, Switzerland) were maintained in MucilAir^{TM} culture medium (Epithelix) as
410 recommended by the manufacturer.
411
412 **Plant collection and extraction**

413 The aerial part of *Hypericum perforatum* L. was collected in the Lille metropolis (France),
414 deposited and identified at the Herbarium of the University of Lille by Gabriel Lefèvre and
415 Céline Rivière. The plant was dried at 37°C for 48 to 72 h. After being powdered, the plant
416 material was extracted three times with methanol for 24 h under agitation. The combined
417 methanolic extract was then concentrated under reduced pressure with a rotary evaporator
418 (Heidolph™, Grosseron, Germany). The obtained crude methanolic extract was then
419 resuspended with DMSO at the concentration of 50 mg/mL for the experiments.
420
421 **Virus**
422 HCoV-229E-luc was kindly gifted by Volker Thiel (60). SARS-CoV-2 variants (the original Wuhan
423 strain (EPI_ISL_410720), the alpha (B1.1.7; EPI_ISL_1653931) and omicron variants (B1.1.529;
424 EPI_ISL_7696645). The original strain was kindly provided by the French National Reference
425 Center for Respiratory Viruses hosted by Institut Pasteur (Paris, France). SARS-CoV strain
426 (Frankfurt isolate) was provided by Dr Michelle Vialette (Unité de Sécurité Microbiologique).
427 MERS-CoV was recovered by transfecting the infectious clone of MERS-CoV-EMC12 (kindly
428 provided by Luis Enjuanes) in Huh-7 cells.
429
430 **Cell viability**
431 Huh-7 or Vero-81 cells were seeded in 96-well plate at a density of $1x10^4$ and $1.5x10^4$ cells per
432 well respectively, and incubated for 24 h at 37°C and 5% CO_2. A 3-(4,5-dimethylthiazol-2-yl)-
433 5-(3-carboxymethoxyphenyl)-2-(4-sulfophenyl)-2H-tetrazolium (MTS)-based viability assay
434 (CellTiter 96® AQueous One Solution Cell Proliferation Assay, Promega) was performed as
435 previously described (25).
436
437 **MucilAir™ cytoxicity assays**
438 Cytotoxicity was studied according to the manufacturer's instruction either using cytotoxicity
439 LDH assay kit-WST (Dojindo) or by measuring transepithelial electrical resistance (TEER)
440 (Millicell® ERS-2, Millipore) as previously described (25). Toxicity is considered when LDH
441 secretion is above 5% and TEER below 100 $\Omega.cm^2$.
442
443 **HCoVs infection assays**
444

445 *HCoV-229E-Luc*

446 $2x10^4$ Huh-7/TMPRSS2 cells per well were seeded into a 96-well plate 24 h before infection.
447 Cells were inoculated with HCoV-229E-Luc and, simultaneously, increased concentrations of
448 compound or the plant extract were added to cell culture medium. The inoculum was
449 removed after 1 h and replaced with culture medium containing the compound or the plant
450 extract. The cells were then lysed 7 h later in 20 µl of Renilla luciferase assay lysis buffer
451 (Promega), and luciferase activity was quantified using a Tristar LB 941 luminometer (Berthold
452 Technologies, Bad Bildbad, Germany) as recommended by the manufacturer.

453

454 *MERS-CoV and SARS-CoV*

455 $2x10^5$ Calu-3 or Vero-81/TMPRSS2 cells were seeded in a 24-well plate on coverslips, 48 h or
456 24 h prior infection with MERS-CoV or SARS-CoV, respectively. Cells were inoculated with the
457 virus at a multiplicity of infection (MOI) of 0.1, in the presence of increased concentrations of
458 the compound, for 1 h at 37°C and 5% of CO_2. The inoculum was replaced by culture medium
459 containing the compound and the cells were incubated for 16 h. Supernatants were collected
460 for viral titration and cells were fixed twice with 4% of paraformaldehyde (PFA) before exiting
461 the BSL-3 facility and processed for immunostaining.

462

463 *SARS-CoV-2*

464 $1x10^5$ Vero-81/TMPRSS2 or A549/ACE2 cells per well were seeded in a 48-well plate 24 h
465 before infection. Cells were inoculated with the virus at a MOI of 0.3, in the presence of
466 increased concentration of the compound, for 1 h at 37°C and 5% of CO_2. 50 nM tariquidar, a
467 P-glycoprotein inhibitor, was added in the media to inhibit pump efflux, and 10 µM
468 chloroquine was used as a control of the expression of TMPRSS2. Inoculum was replaced with
469 media containing the different compounds and cells were incubated for 16 h at 37°C and 5%
470 of CO_2. The supernatants were collected for viral titration and the cells were lysed using
471 reducing Laëmmli loading buffer for western blot analysis. The samples were inactivated 30
472 min at 95°C.

473

474 **Light-dependent assay**

475 Cells were inoculated with HCoV-229E-Luc, treated with increasing concentrations of the
476 compound and incubated in the cabinet under light or dark conditions before being place in

477 the incubator at 37°C and 5% CO_2. For the light condition, the plate was incubated for 10 min
478 under the light of the safety cabinet. For the dark condition, the experiment was conducted
479 in the dark, with the light of the safety cabinet turned off, and the tubes and plate were
480 covered with aluminum foil. Only the light from the hood next to the safety cabinet was on.
481 After 7 h of incubation, cells were lysed and infection was studied by measuring the luciferase
482 activity.
483
484 **Infectivity titration**
485 Huh-7 (MERS-CoV) or Vero-E6 (SARS-CoV and SARS-CoV-2) were seeded in a 96-well plate and
486 were inoculated with 1/10 serially diluted supernatants. After 5 days (SARS-CoV and SARS-
487 CoV-2) or 7 days (MERS-CoV) of incubation at 37°C and 5% of CO_2, the 50% tissue culture
488 infectious dose (TCID50/mL) was determined by assessing the virus-induced cytopathic effect
489 and using the Spearman-Kärber formula.
490
491 **Western blot detection**
492 Proteins were separated onto a 12% SDS-polyacrylamide gel electrophoresis and transferred
493 on nitrocellulose membranes (Hybond-ECL, Amersham). The membranes were blocked and
494 incubated overnight at 4°C with a polyclonal rabbit anti-SARS-CoV-2 nucleocapsid antibody
495 (1/4000), a mouse anti-ß-tubulin (1/4000) or a rabbit anti-HO-1 (1/1000). They were visualized
496 by enhanced chemoluminescence (Pierce™ ECL, ThermoFisher Scientific) on LAS3000
497 (Fujifilm) or Amersham ImageQuant 800 (Cytiva).
498
499 **Immunostaining**
500 Cells were permeabilized for 5 min with 0.4 % Triton X-100 and blocked with 5% of goat serum
501 for 30 min and were incubated with anti-dsRNA monoclonal mouse antibody (clone J2) or anti-
502 MERS-CoV Spike protein polyclonal rabbit antibody. Cells were rinsed three times with PBS,
503 and immunostained with an Alexa 594-conjugated goat anti-rabbit secondary antibody or an
504 alexa-488-conjugated donkey anti-mouse secondary antibody and DAPI. The coverslips were
505 mounted on microscope slides in Mowiol. The images were acquired with an Evos M5000
506 microscope (Thermo Fischer Scientific). Ten images were randomly taken for each condition
507 in duplicate. The number of cells were determined by the number of nuclei, and infected cells
508 were detected by quantifying the number of dsRNA-positive or Spike-positive cells.

509

510 **MucilAir™-Human airway epithelia (MucilAir™-HAE) infection assay**

511 The apical surface of the cells was rinsed 3 times for 10 min using MucilAir™-HAE culture
512 medium to remove the mucosal secretion. The cells were inoculated at the apical side with
513 HCoV-229E-Luc (MOI = 0.01) or SARS-CoV-2 (MOI = 0.3) and treated with 4 µM or 12 µM or
514 HF or 0.025% DMSO for 1 h. On the apical pole, the inoculum was removed and replaced by
515 10 µL of medium containing the compounds. Simultaneously, HF or DMSO were added in the
516 basolateral medium.

517 For HCoV-229E-Luc infection, after 24 h of incubation, 140 µL of culture medium was added
518 on the apical surface of MucilAir™-HAE and collected for RNA extraction. The cells were then
519 lysed with 40 µL of Renilla luciferase assay lysis buffer (Promega). Luciferase activity was
520 quantified as previously described.

521 For SARS-CoV-2 infection, after 48 h of incubation, 140 µL of culture medium was added on
522 the apical surface of MucilAir™-HAE and was collected for RNA extraction and viral titration.
523 The cells were lysed and RNA was extracted for RT-qPCR assay.

524

525 **RT-qPCR assay**

526 RNA was extracted from MucilAir™-HAE supernatants or cells using QIAamp Viral RNA Mini
527 kit (Qiagen) and NucleoSpin RNA plus (Macherey Nagel) respectively. One-step qPCR assay
528 was performed using 5 µL of RNA and Takyon Low rox one-step RT probe master mix (UFD-
529 LPRT-C0101, Eurogentec) with specific primers and probes (**Supplemental Table 1**) and using
530 a Quantstudio 3 (Applied Biosystems). The expressions of HCoV-229E M gene and SARS-CoV-
531 2 E gene were quantified using a standard curve.

532

533 **Time-of-addition assay**

534 One day prior the infection, $1x10^5$ Vero-81/TMPRSS2 cells per well and $2x10^4$ Huh-7/TMPRSS2
535 cells per well were seeded into a 48-well plate or 96-well plate for SARS-CoV-2 or HCoV-229E-
536 Luc infection, respectively. To assess which viral step is inhibited, the different compounds
537 were added at different time points, either 1 h before the inoculation (corresponding to the
538 condition “pre-treatment”), or during the inoculation or 1 h, 2 h, 3 h after the inoculation (1 h
539 p.i., 2 h p.i. or 3 h p.i.). The cells were then lysed at 16 h or 7 h post-infection for SARS-CoV-2
540 or HCoV-229E-Luc, respectively, and analyzed as described ahead.

541

542 **Pseudotyped particle entry assay**

543 Particles pseudotyped with either the spike protein of SARS-CoV-2 (SARS2pp), or HCoV-229E
544 (HCoV-229Epp), were produced as previously described (61). $4.5x10^3$ HEK293TT/ACE2
545 (SARS2pp) cells per well or $1x10^4$ Huh-7/TMPRSS2 (229Epp) cells per well were seeded into a
546 96-well plate 24 h before infection. Cells were inoculated with SARS2pp and 229Epp in the
547 presence of HF or HC (2.5, 5 or 10 µM) for 2 h at 37°C and 5% of CO_2. The inoculum was
548 removed and replaced with culture media without compound. The cells were lysed after 48 h
549 of incubation. The luciferase activity was then measured with Firefly luciferase assay kit
550 (Promega) according to the manufacturer recommendations and using a luminometer
551 (Berthold).

552

553 **Drug combination assay**

554 24 h before infection, $4.5x10^3$ F1G-Red cells per well were seeded in 384-well plate in DMEM
555 with 2% of FBS. Compounds (HF, remdesivir and nirmatrelvir) were dissolved in DMSO at
556 concentrations stocks of 10 or 100 nM. 1 h before infection, dose-response concentrations of
557 the compound (seven- 2-fold serial dilutions) were dispensed onto the cells using an Echo 550
558 acoustic dispenser (Labcyte) in three biological replicates. Last column of each plate contained
559 DMSO control solvent. DMSO was distributed at equivalent volumes as negative control. The
560 cells were then inoculated with the virus by adding 10 µL of inoculum (MOI = 0.3) and 50 nM
561 tariquidar for 16 h. The infection was assessed by using an IN CELL Analyzer 6500 high-
562 throughput automated confocal microscope (Ge Healthcare) located in BSL-3 safety
563 laboratory. Nine images were taken (20X objective, NA 0.75) for each condition and the
564 number of infected cells was quantified using Columbus image analysis software (Perkin
565 Elmer). The data were analyzed and we used Synergy Finder
566 (http://www.synergyfinderplus.org/) for the calculation of the synergy scores (mean and *p*-
567 value) and https://synergyfinder.fimm.fi/ for the most synergistic area (MSA).

568

569 **RNA interference**

570 Cells were transfected with small interfering RNA (siRNA) targeting HO-1 (siHO-1, final
571 concentration: 10 nM) (Gene HMOX1, AM16708, Assay ID 11056, ThermoFischer) or with a
572 non-targeting siRNA control (siCTRL, Dharmacon) using Lipofectamine RNAi MAX (Invitrogen)

573 according to manufacturer's recommendations. After 24 h of incubation, cells were treated
574 with increasing concentration of hemin or HF, infected or not with HCoV-229E-Luc and
575 incubated again for 24 h. Cells were then lysed using Laëmmli buffer in reducing conditions or
576 with the Renilla luciferase assay lysis buffer. HO-1 expression was then studied by Western
577 Blot.
578
579 **Statistical analysis and IC_{50} and CC_{50} calculation**
580 IC_{50} and CC_{50} values were calculated by nonlinear regression curve fitting with variable slopes
581 and mean and standard error of the mean (SEM) values were graphed using GraphPad Prism
582 software version 10.0.3 (Boston, Ma, USA) and by constraining the top to 100% and the
583 bottom to 0%. Statistical analysis was performed using Mann-Whitney non-parametric test by
584 comparing each treated group with the untreated control (DMSO control). *P*-values < 0.05
585 were considered significantly different from the control.
586
587
588 **ACKNOWLEDGMENTS**
589 We are grateful for the technical help of Robin Prath and Nicolas Vandenabeele in the
590 BSL-3 facility. We also thank the team of Fernando Real, especially Cyrine Bentaleb for useful
591 discussions. We also would like to thank Steve Polyak for his advices on combination assays.
592 Finally, we would like to thank Yves Rouillé for kindly supplying F1G-Red cell line. We thank
593 Lola Dandoy for technical help.
594 This project was funded by Région Hauts-de-France and I-Site (FlavoCoV project) and
595 CNRS (VIROCRIB project). We thank the Fédération Hospitalo-Universitaire (FHU) RESPIRE for
596 financial support.
597 I.R. is a recipient of a Health-PhD fellowship. L.D. is a recipient of a CNRS and Institut
598 Pasteur de Lille fellowship.
599
600
601 **REFERENCES**
602 1. Owen DR, Allerton CMN, Anderson AS, Aschenbrenner L, Avery M, Berritt S, Boras B,
603 Cardin RD, Carlo A, Coffman KJ, Dantonio A, Di L, Eng H, Ferre R, Gajiwala KS, Gibson
604 SA, Greasley SE, Hurst BL, Kadar EP, Kalgutkar AS, Lee JC, Lee J, Liu W, Mason SW,

605 Noell S, Novak JJ, Obach RS, Ogilvie K, Patel NC, Pettersson M, Rai DK, Reese MR,
606 Sammons MF, Sathish JG, Singh RSP, Steppan CM, Stewart AE, Tuttle JB, Updyke L,
607 Verhoest PR, Wei L, Yang Q, Zhu Y. 2021. An oral SARS-CoV-2 Mpro inhibitor clinical
608 candidate for the treatment of COVID-19. Science 374:1586–1593.
609 2. Lamb YN. 2022. Nirmatrelvir Plus Ritonavir: First Approval. Drugs 82:585–591.
610 3. Warren TK, Jordan R, Lo MK, Ray AS, Mackman RL, Soloveva V, Siegel D, Perron M,
611 Bannister R, Hui HC, Larson N, Strickley R, Wells J, Stuthman KS, Van Tongeren SA,
612 Garza NL, Donnelly G, Shurtleff AC, Retterer CJ, Gharaibeh D, Zamani R, Kenny T, Eaton
613 BP, Grimes E, Welch LS, Gomba L, Wilhelmsen CL, Nichols DK, Nuss JE, Nagle ER,
614 Kugelman JR, Palacios G, Doerffler E, Neville S, Carra E, Clarke MO, Zhang L, Lew W,
615 Ross B, Wang Q, Chun K, Wolfe L, Babusis D, Park Y, Stray KM, Trancheva I, Feng JY,
616 Barauskas O, Xu Y, Wong P, Braun MR, Flint M, McMullan LK, Chen S-S, Fearns R,
617 Swaminathan S, Mayers DL, Spiropoulou CF, Lee WA, Nichol ST, Cihlar T, Bavari S.
618 2016. Therapeutic efficacy of the small molecule GS-5734 against Ebola virus in rhesus
619 monkeys. Nature 531:381–385.
620 4. Agostini ML, Andres EL, Sims AC, Graham RL, Sheahan TP, Lu X, Smith EC, Case JB,
621 Feng JY, Jordan R, Ray AS, Cihlar T, Siegel D, Mackman RL, Clarke MO, Baric RS,
622 Denison MR. 2018. Coronavirus Susceptibility to the Antiviral Remdesivir (GS-5734) Is
623 Mediated by the Viral Polymerase and the Proofreading Exoribonuclease. mBio
624 9:10.1128/mbio.00221-18.
625 5. Beigel JH, Tomashek KM, Dodd LE, Mehta AK, Zingman BS, Kalil AC, Hohmann E, Chu
626 HY, Luetkemeyer A, Kline S, Lopez de Castilla D, Finberg RW, Dierberg K, Tapson V,
627 Hsieh L, Patterson TF, Paredes R, Sweeney DA, Short WR, Touloumi G, Lye DC,
628 Ohmagari N, Oh M-D, Ruiz-Palacios GM, Benfield T, Fätkenheuer G, Kortepeter MG,
629 Atmar RL, Creech CB, Lundgren J, Babiker AG, Pett S, Neaton JD, Burgess TH, Bonnett
630 T, Green M, Makowski M, Osinusi A, Nayak S, Lane HC, ACTT-1 Study Group Members.
631 2020. Remdesivir for the Treatment of Covid-19 - Final Report. N Engl J Med 383:1813–
632 1826.
633 6. Yin W, Mao C, Luan X, Shen D-D, Shen Q, Su H, Wang X, Zhou F, Zhao W, Gao M,
634 Chang S, Xie Y-C, Tian G, Jiang H-W, Tao S-C, Shen J, Jiang Y, Jiang H, Xu Y, Zhang
635 S, Zhang Y, Xu HE. 2020. Structural basis for inhibition of the RNA-dependent RNA
636 polymerase from SARS-CoV-2 by remdesivir. Science 368:1499–1504.
637 7. Sheahan TP, Sims AC, Zhou S, Graham RL, Pruijssers AJ, Agostini ML, Leist SR, Schäfer
638 A, Dinnon KH, Stevens LJ, Chappell JD, Lu X, Hughes TM, George AS, Hill CS,

639 Montgomery SA, Brown AJ, Bluemling GR, Natchus MG, Saindane M, Kolykhalov AA,
640 Painter G, Harcourt J, Tamin A, Thornburg NJ, Swanstrom R, Denison MR, Baric RS.
641 2020. An orally bioavailable broad-spectrum antiviral inhibits SARS-CoV-2 in human
642 airway epithelial cell cultures and multiple coronaviruses in mice. Science Translational
643 Medicine 12:eabb5883.
644 8. Stuyver LJ, Whitaker T, McBrayer TR, Hernandez-Santiago BI, Lostia S, Tharnish PM,
645 Ramesh M, Chu CK, Jordan R, Shi J, Rachakonda S, Watanabe KA, Otto MJ, Schinazi
646 RF. 2003. Ribonucleoside Analogue That Blocks Replication of Bovine Viral Diarrhea and
647 Hepatitis C Viruses in Culture. Antimicrobial Agents and Chemotherapy 47:244–254.
648 9. Uraki R, Ito M, Kiso M, Yamayoshi S, Iwatsuki-Horimoto K, Furusawa Y, Sakai-Tagawa
649 Y, Imai M, Koga M, Yamamoto S, Adachi E, Saito M, Tsutsumi T, Otani A, Kikuchi T,
650 Yotsuyanagi H, Halfmann PJ, Pekosz A, Kawaoka Y. 2023. Antiviral and bivalent vaccine
651 efficacy against an omicron XBB.1.5 isolate. Lancet Infect Dis 23:402–403.
652 10. Imai M, Ito M, Kiso M, Yamayoshi S, Uraki R, Fukushi S, Watanabe S, Suzuki T, Maeda
653 K, Sakai-Tagawa Y, Iwatsuki-Horimoto K, Halfmann PJ, Kawaoka Y. 2023. Efficacy of
654 Antiviral Agents against Omicron Subvariants BQ.1.1 and XBB. N Engl J Med 388:89–
655 91.
656 11. Bez P, D'ippolito G, Deiana CM, Finco Gambier R, Pica A, Costanzo G, Garzi G, Scarpa
657 R, Landini N, Cinetto F, Firinu D, Milito C. 2023. Struggling with COVID-19 in Adult
658 Inborn Errors of Immunity Patients: A Case Series of Combination Therapy and Multiple
659 Lines of Therapy for Selected Patients. 7. Life 13:1530.
660 12. Baldi F, Dentone C, Mikulska M, Fenoglio D, Mirabella M, Magnè F, Portunato F,
661 Altosole T, Sepulcri C, Giacobbe DR, Uras C, Scavone G, Taramasso L, Orsi A, Cittadini
662 G, Filaci G, Bassetti M. 2023. Case report: Sotrovimab, remdesivir and
663 nirmatrelvir/ritonavir combination as salvage treatment option in two
664 immunocompromised patients hospitalized for COVID-19. Frontiers in Medicine 9.
665 13. Brown L-AK, Moran E, Goodman A, Baxendale H, Bermingham W, Buckland M,
666 AbdulKhaliq I, Jarvis H, Hunter M, Karanam S, Patel A, Jenkins M, Robbins A, Khan S,
667 Simpson T, Jolles S, Underwood J, Savic S, Richter A, Shields A, Brown M, Lowe DM.
668 2022. Treatment of chronic or relapsing COVID-19 in immunodeficiency. Journal of
669 Allergy and Clinical Immunology 149:557-561.e1.
670 14. Anderson AS, Caubel P, Rusnak JM, EPIC-HR Trial Investigators. 2022. Nirmatrelvir-
671 Ritonavir and Viral Load Rebound in Covid-19. N Engl J Med 387:1047–1049.
672 15. Charness ME, Gupta K, Stack G, Strymish J, Adams E, Lindy DC, Mohri H, Ho DD. 2022.

673 Rebound of SARS-CoV-2 Infection after Nirmatrelvir–Ritonavir Treatment. N Engl J Med
674 387:1045–1047.
675 16. EMA. 2023. Lagevrio: Withdrawn application. European Medicines Agency. Text.
676 https://www.ema.europa.eu/en/medicines/human/withdrawn-applications/lagevrio.
677 Retrieved 22 September 2023.
678 17. Zhou S, Hill CS, Sarkar S, Tse LV, Woodburn BMD, Schinazi RF, Sheahan TP, Baric RS,
679 Heise MT, Swanstrom R. 2021. β-d-N4-hydroxycytidine Inhibits SARS-CoV-2 Through
680 Lethal Mutagenesis But Is Also Mutagenic To Mammalian Cells. J Infect Dis 224:415–
681 419.
682 18. Coronaviridae Study Group of the International Committee on Taxonomy of Viruses. 2020.
683 The species Severe acute respiratory syndrome-related coronavirus: classifying 2019-
684 nCoV and naming it SARS-CoV-2. Nat Microbiol 5:536–544.
685 19. Tang G, Liu Z, Chen D. 2022. Human coronaviruses: Origin, host and receptor. Journal of
686 Clinical Virology 155:105246.
687 20. Belouzard S, Millet JK, Licitra BN, Whittaker GR. 2012. Mechanisms of Coronavirus Cell
688 Entry Mediated by the Viral Spike Protein. Viruses 4:1011–1033.
689 21. Jackson CB, Farzan M, Chen B, Choe H. 2022. Mechanisms of SARS-CoV-2 entry into
690 cells. Nat Rev Mol Cell Biol 23:3–20.
691 22. Hoffmann M, Pöhlmann S. 2021. How SARS-CoV-2 makes the cut. Nat Microbiol 6:828–
692 829.
693 23. Weiss SR, Leibowitz JL. 2011. Coronavirus Pathogenesis. Adv Virus Res 81:85–164.
694 24. Denaro M, Smeriglio A, Barreca D, De Francesco C, Occhiuto C, Milano G, Trombetta D.
695 2020. Antiviral activity of plants and their isolated bioactive compounds: An update.
696 Phytother Res 34:742–768.
697 25. Meunier T, Desmarets L, Bordage S, Bamba M, Hervouet K, Rouillé Y, François N,
698 Decossas M, Sencio V, Trottein F, Tra Bi FH, Lambert O, Dubuisson J, Belouzard S,
699 Sahpaz S, Séron K. 2022. A Photoactivable Natural Product with Broad Antiviral Activity
700 against Enveloped Viruses, Including Highly Pathogenic Coronaviruses. Antimicrob
701 Agents Chemother 66:e0158121.
702 26. Millet JK, Séron K, Labitt RN, Danneels A, Palmer KE, Whittaker GR, Dubuisson J,
703 Belouzard S. 2016. Middle East respiratory syndrome coronavirus infection is inhibited by
704 griffithsin. Antiviral Res 133:1–8.
705 27. Al Ibrahim M, Akissi ZLE, Desmarets L, Lefèvre G, Samaillie J, Raczkiewicz I, Sahpaz
706 S, Dubuisson J, Belouzard S, Rivière C, Séron K. 2023. Discovery of Anti-Coronavirus

Cinnamoyl Triterpenoids Isolated from Hippophae rhamnoides during a Screening of Halophytes from the North Sea and Channel Coasts in Northern France. Int J Mol Sci 24:16617.

28. Hypericum Tourn. ex L. | Plants of the World Online | Kew Science. Plants of the World Online. http://powo.science.kew.org/taxon/urn:lsid:ipni.org:names:30002180-2. Retrieved 18 November 2022.
29. de Carvalho Meirelles G, Bridi H, von Poser GL, Nemitz MC. 2019. Hypericum species: An analysis on the patent technologies. Fitoterapia 139:104363.
30. Butterweck V, Schmidt M. 2007. St. John's wort: role of active compounds for its mechanism of action and efficacy. Wien Med Wochenschr 157:356–361.
31. EMA. 2023. Hyperici herba. European Medicines Agency. Text. https://www.ema.europa.eu/en/medicines/herbal/hyperici-herba-0. Retrieved 9 April 2024.
32. Röder C, Schaefer M, Leucht S. 2004. [Meta-analysis of effectiveness and tolerability of treatment of mild to moderate depression with St. John's Wort]. Fortschr Neurol Psychiatr 72:330–343.
33. Linde K, Berner MM, Kriston L. 2008. St John's wort for major depression. Cochrane Database Syst Rev 2008:CD000448.
34. Kubin A, Wierrani F, Burner U, Alth G, Grünberger W. 2005. Hypericin--the facts about a controversial agent. Curr Pharm Des 11:233–253.
35. Lopez-Bazzocchi I, Hudson JB, Towers GHN. 1991. Antiviral Activity of the Photoactive Plant Pigment Hypericin. Photochemistry and Photobiology 54:95–98.
36. Mohamed FF, Anhlan D, Schöfbänker M, Schreiber A, Classen N, Hensel A, Hempel G, Scholz W, Kühn J, Hrincius ER, Ludwig S. 2022. Hypericum perforatum and Its Ingredients Hypericin and Pseudohypericin Demonstrate an Antiviral Activity against SARS-CoV-2. Pharmaceuticals (Basel) 15:530.
37. Jendželovská Z, Jendželovský R, Kuchárová B, Fedoročko P. 2016. Hypericin in the Light and in the Dark: Two Sides of the Same Coin. Front Plant Sci 7:560.
38. Desmarets L, Callens N, Hoffmann E, Danneels A, Lavie M, Couturier C, Dubuisson J, Belouzard S, Rouillé Y. 2022. A reporter cell line for the automated quantification of SARS-CoV-2 infection in living cells. Front Microbiol 13:1031204.
39. Cardile A, Passarini C, Zanrè V, Fiore A, Menegazzi M. 2023. Hyperforin Enhances Heme Oxygenase-1 Expression Triggering Lipid Peroxidation in BRAF-Mutated Melanoma Cells and Hampers the Expression of Pro-Metastatic Markers. Antioxidants (Basel)

741 12:1369.
742 40. Kim D-H, Ahn H-S, Go H-J, Kim D-Y, Kim J-H, Lee J-B, Park S-Y, Song C-S, Lee S-W,
743 Ha S-D, Choi C, Choi I-S. 2021. Hemin as a novel candidate for treating COVID-19 via
744 heme oxygenase-1 induction. Sci Rep 11:21462.
745 41. Espinoza JA, González PA, Kalergis AM. 2017. Modulation of Antiviral Immunity by
746 Heme Oxygenase-1. Am J Pathol 187:487–493.
747 42. Maridass M, Britto AD. 2008. Origins of Plant Derived Medicines. Ethnobotanical Leaflets
748 2008.
749 43. Wang L, Zhang R-M, Liu G-Y, Wei B-L, Wang Y, Cai H-Y, Li F-S, Xu Y-L, Zheng S-P,
750 Wang G. 2010. Chinese herbs in treatment of influenza: A randomized, double-blind,
751 placebo-controlled trial. Respiratory Medicine 104:1362–1369.
752 44. Adel Mehraban MS, Shirzad M, Mohammad Taghizadeh Kashani L, Ahmadian-Attari
753 MM, Safari AA, Ansari N, Hatami H, Kamalinejad M. 2023. Efficacy and safety of add-
754 on Viola odorata L. in the treatment of COVID-19: A randomized double-blind controlled
755 trial. J Ethnopharmacol 304:116058.
756 45. Wilson D, Goggin K, Williams K, Gerkovich MM, Gqaleni N, Syce J, Bartman P, Johnson
757 Q, Folk WR. 2015. Consumption of Sutherlandia frutescens by HIV-Seropositive South
758 African Adults: An Adaptive Double-Blind Randomized Placebo Controlled Trial. PLoS
759 One 10:e0128522.
760 46. Hudson JB, Lopez-Bazzocchi I, Towers GH. 1991. Antiviral activities of hypericin.
761 Antiviral Res 15:101–112.
762 47. Barnes J, Anderson LA, Phillipson JD. 2001. St John's wort (Hypericum perforatum L.):
763 a review of its chemistry, pharmacology and clinical properties. J Pharm Pharmacol
764 53:583–600.
765 48. Biber A, Fischer H, Römer A, Chatterjee SS. 1998. Oral bioavailability of hyperforin from
766 hypericum extracts in rats and human volunteers. Pharmacopsychiatry 31 Suppl 1:36–43.
767 49. Hatanaka J, Shinme Y, Kuriyama K, Uchida A, Kou K, Uchida S, Yamada S, Onoue S.
768 2011. In vitro and in vivo characterization of new formulations of St. John's Wort extract
769 with improved pharmacokinetics and anti-nociceptive effect. Drug Metab Pharmacokinet
770 26:551–558.
771 50. Agrosí M, Mischiatti S, Harrasser PC, Savio D. 2000. Oral bioavailability of active
772 principles from herbal products in humans. A study on *Hypericum perforatum* extracts
773 using the soft gelatin capsule technology. Phytomedicine 7:455–462.
774 51. Negreş S, Scutari C, Ionică FE, Gonciar V, Velescu BŞ, Şeremet OC, Zanfirescu A,

775 Zbârcea CE, Ştefănescu E, Ciobotaru E, ChiriŢă C. 2016. Influence of hyperforin on the
776 morphology of internal organs and biochemical parameters, in experimental model in mice.
777 Rom J Morphol Embryol 57:663–673.
778 52. Donà M, Dell'Aica I, Pezzato E, Sartor L, Calabrese F, Barbera MD, Donella-Deana A,
779 Appendino G, Borsarini A, Caniato R, Garbisa S. 2004. Hyperforin Inhibits Cancer
780 Invasion and Metastasis. Cancer Research 64:6225–6232.
781 53. Hill-Batorski L, Halfmann P, Neumann G, Kawaoka Y. 2013. The cytoprotective enzyme
782 heme oxygenase-1 suppresses Ebola virus replication. J Virol 87:13795–13802.
783 54. Zhu Z, Wilson AT, Mathis MM, Wen F, Brown KE, Luxon BA, Schmidt WN. 2008. Heme
784 Oxygenase-1 suppresses Hepatitis C Virus replication and increases resistance of
785 hepatocytes to oxidant injury. Hepatology 48:1430–1439.
786 55. Tseng C-K, Lin C-K, Wu Y-H, Chen Y-H, Chen W-C, Young K-C, Lee J-C. 2016. Human
787 heme oxygenase 1 is a potential host cell factor against dengue virus replication. 1. Sci Rep
788 6:32176.
789 56. Ibáñez FJ, Farías MA, Retamal-Díaz A, Espinoza JA, Kalergis AM, González PA. 2017.
790 Pharmacological Induction of Heme Oxygenase-1 Impairs Nuclear Accumulation of
791 Herpes Simplex Virus Capsids upon Infection. Front Microbiol 8:2108.
792 57. Li W, Shi Z, Yu M, Ren W, Smith C, Epstein JH, Wang H, Crameri G, Hu Z, Zhang H,
793 Zhang J, McEachern J, Field H, Daszak P, Eaton BT, Zhang S, Wang L-F. 2005. Bats are
794 natural reservoirs of SARS-like coronaviruses. Science 310:676–679.
795 58. Temmam S, Vongphayloth K, Baquero E, Munier S, Bonomi M, Regnault B,
796 Douangboubpha B, Karami Y, Chrétien D, Sanamxay D, Xayaphet V, Paphaphanh P,
797 Lacoste V, Somlor S, Lakeomany K, Phommavanh N, Pérot P, Dehan O, Amara F, Donati
798 F, Bigot T, Nilges M, Rey FA, van der Werf S, Brey PT, Eloit M. 2022. Bat coronaviruses
799 related to SARS-CoV-2 and infectious for human cells. Nature 604:330–336.
800 59. Lavie M, Dubuisson J, Belouzard S. 2022. SARS-CoV-2 Spike Furin Cleavage Site and
801 S2' Basic Residues Modulate the Entry Process in a Host Cell-Dependent Manner. J Virol
802 96:e0047422.
803 60. van den Worm SHE, Eriksson KK, Zevenhoven JC, Weber F, Züst R, Kuri T, Dijkman R,
804 Chang G, Siddell SG, Snijder EJ, Thiel V, Davidson AD. 2012. Reverse genetics of SARS-
805 related coronavirus using vaccinia virus-based recombination. PLoS One 7:e32857.
806 61. Belouzard S, Chu VC, Whittaker GR. 2009. Activation of the SARS coronavirus spike
807 protein via sequential proteolytic cleavage at two distinct sites. Proc Natl Acad Sci U S A
808 106:5871–5876.

809

810 **FIGURES**

811

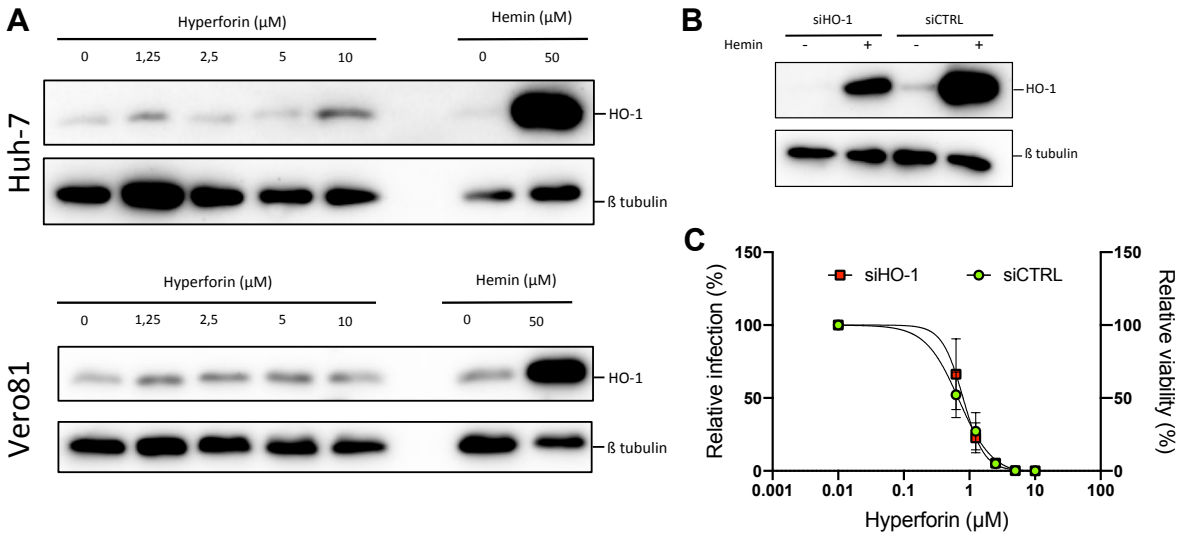

812

813 **Figure 1. The antiviral activity of HF is not linked with HO-1 pathway**. **A)** Huh-7 cells or Vero81 cells
814 were treated with increasing concentrations of HF. HO-1 expression was then studied by Western Blot.
815 **B)** Huh-7 cells were treated with siRNA targeting HO-1 (siHO-1) or control siRNA (siCTRL). 24 h later,
816 cells were treated or not with 50 µM of hemin. HO-1 expression was then studied by Western Blot. **C)**
817 Dose-response assays of HF against HCoV-229E were performed in presence of siHO-1 or siCTRL. The
818 luciferase activity was measured after 24 h of incubation. Western Blots were representative for 3
819 independent experiments. Data were presented as means +/- SEM of 3 independent experiments
820 performed in triplicates.

821

822

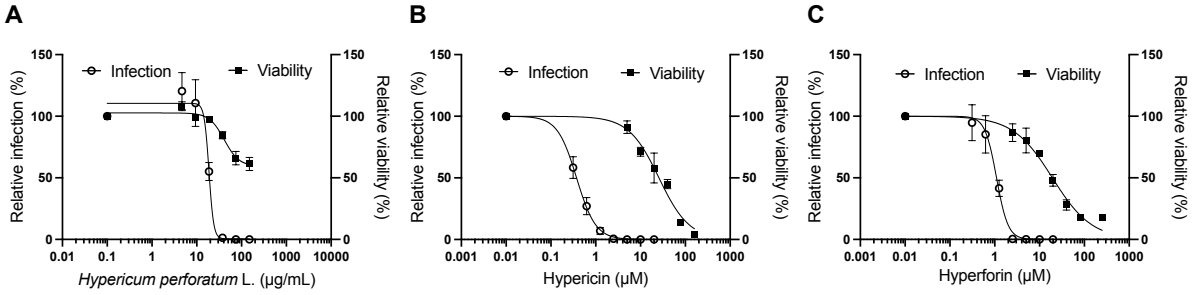

823

824 **Figure 2. Cytotoxicity and antiviral activity of *Hypericum perforatum* L. and its metabolites against**
825 **HCoV-229E**. Huh-7 cells were inoculated with HCoV-229E-Luc in the presence of increasing
826 concentrations of (**A**) *Hypericum perforatum* L. crude methanolic extract, (**B**) HC or (**C**) HF. Cells were
827 lysed 7 h after infection and luciferase activity was quantified. For the cytotoxicity assay, cells were
828 incubated 24 h with increasing concentrations of the crude extract or the molecules and MTS assay
829 were performed. Results are expressed as the means +/- SEM of 3 independent experiments
830 performed in triplicate.

831

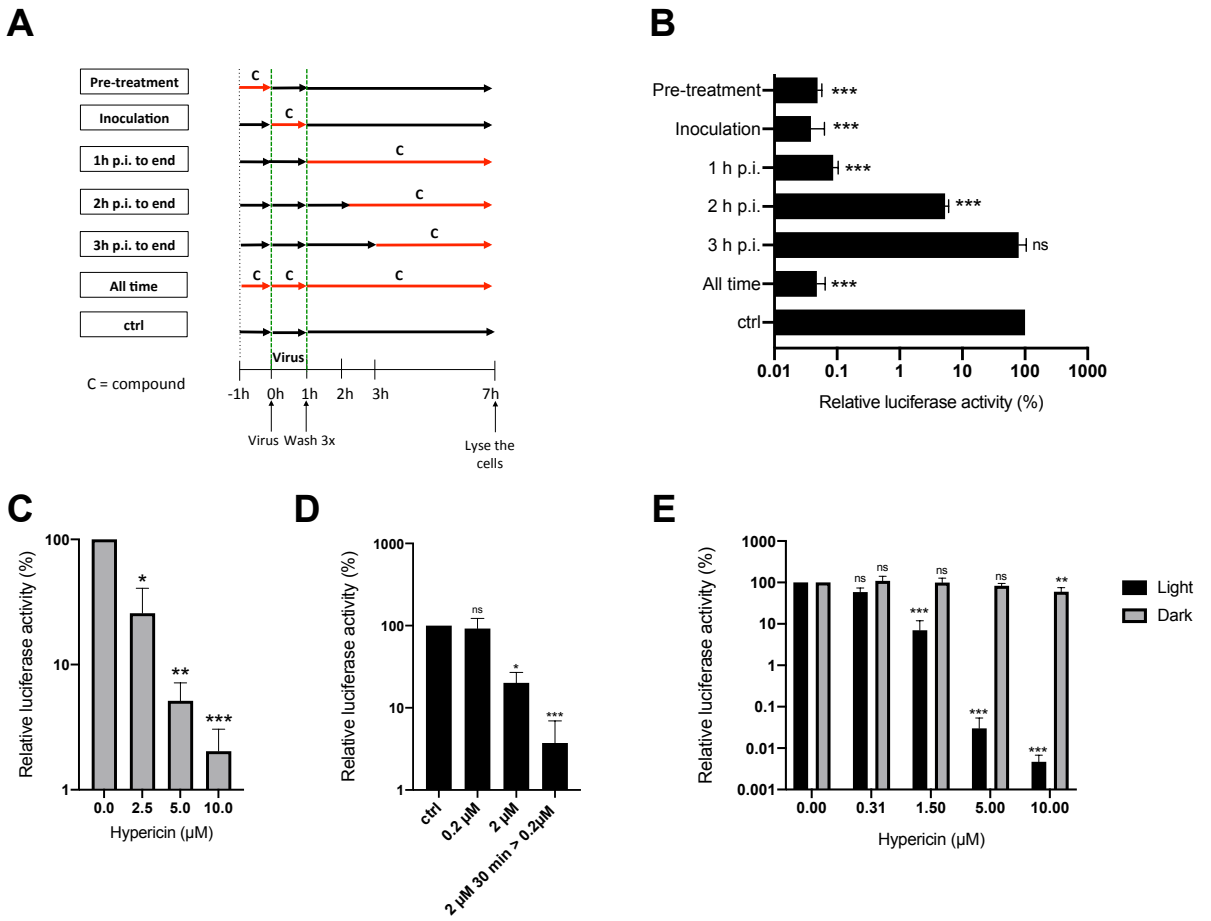

Figure 3. HC inhibits HCoV-229E entry by directly targeting the virus in a light-dependent manner. **A)** Graphical representation of the time-of-addition assay. The compound (C) was added at different time points during infection. **B)** Huh-7/TMPRSS2 cells were inoculated with HCoV-229E in the presence of 4 µM HC at different timepoints. Cells were lysed 7 h p.i. and luciferase activity was quantified. **C)** Huh-7/TMPRSS2 cells were inoculated with 229Epp in the presence of increasing concentrations of HC. After 2 h, the inoculum was removed and replaced with medium without compound for 46 h. Cells were lysed and luciferase activity was quantified. **D)** HCoV-229E-Luc was incubated with 2 µM HC for 30 min and dilute 10 times to reach a concentration of 0.2 µM HC for inoculation of Huh-7/TMPRSS2 cells (2 µM > 0.2 µM). As controls, cells were inoculated with HCoV-229E-Luc in the presence of 0.2 or 2 µM HC. The MOI was the same in all conditions. Cells were lysed 7 h p.i. and luciferase activity was quantified. **E)** Huh-7/TMPRSS2 cells were treated with increasing concentrations of HC and inoculated with HCoV-229E-Luc in dark or light condition. Plates were kept in the dark or exposed to the light for 10 min during inoculation, and 10 min p.i.. Cells were lysed as described and luciferase activity was quantified. Results were expressed as the means +/- SEM of 3 independent experiments performed in triplicate. Statistical analyses were performed using Mann-Whitney non-parametric test; ns: non significative, * $P < 0.05$, ** $P < 0.01$, *** $P < 0.001$. C: compound. p.i.: post inoculation.

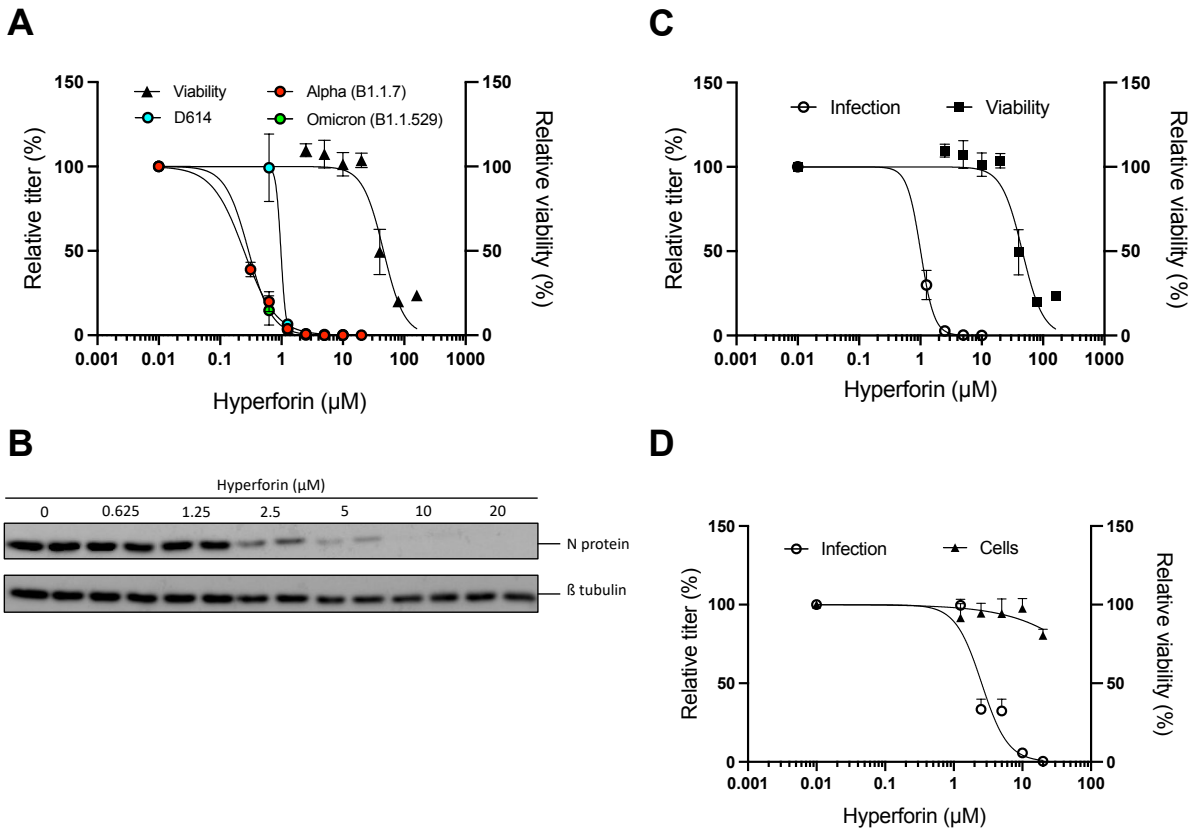

Figure 4. Antiviral activity of HF against several HCoVs. **A)** Vero-81/TMPRSS2 cells were inoculated with different variants of SARS-CoV-2 (D614 strain, alpha or omicron variant) in the presence of increasing concentrations of HF for 16 h. Supernatants were collected, and the viral titers were determined by TCID50/mL. Viability at 24 h was assessed by MTS assay. **B)** A549/ACE2 cells were infected with SARS-CoV-2 alpha variant in the presence of increasing concentrations of HF for 16 h. Cells were lysed and Western Blot analysis was performed. Western blot is representative of 3 independent experiments. **C)** Vero-81/TMPRSS2 cells were inoculated with SARS-CoV in the presence of increasing concentrations of HF for 16 h. Supernatants were collected for viral titration. Viability was determined by MTS assay. **D)** Calu-3 cells were inoculated with MERS-CoV in the presence of increasing concentrations of HF for 16 h. Supernatants were collected for viral titration; Cell number was determined by staining of the nuclei with DAPI. Data were presented as means +/- SEM of 3 independent experiments performed in duplicate (**A, C, D**).

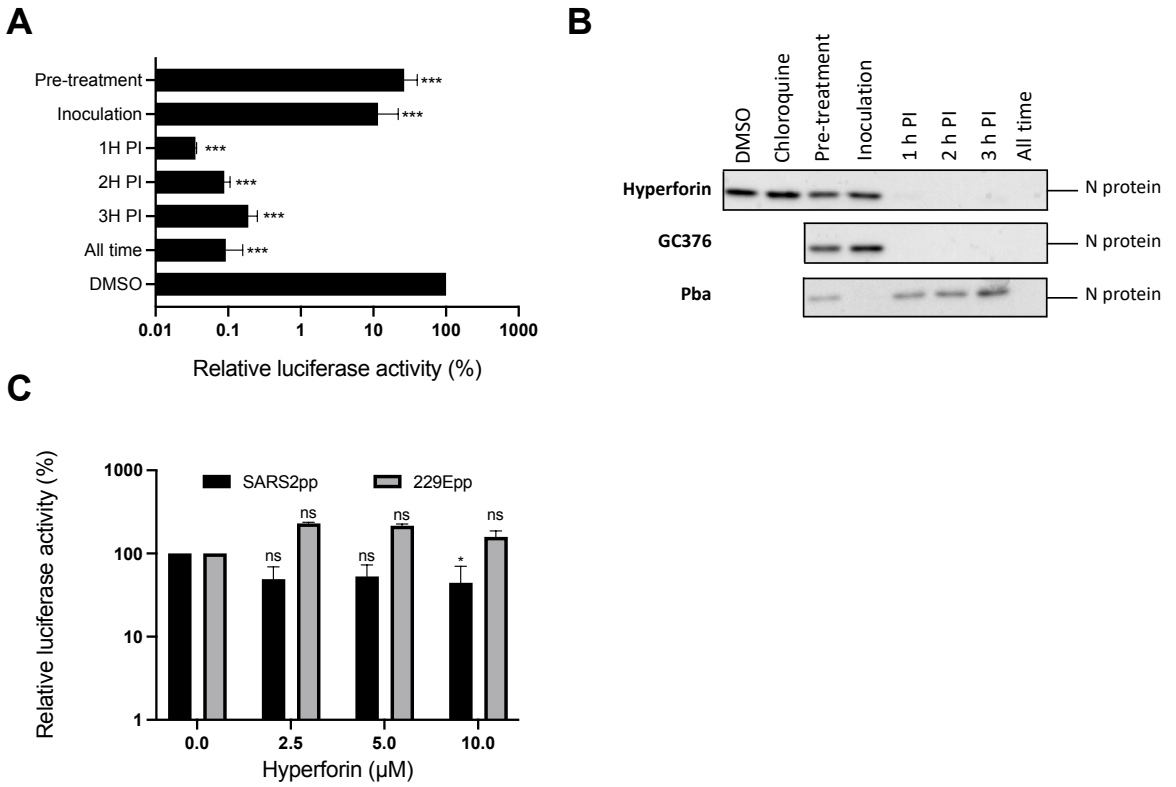

Figure 5. HF inhibits a post-entry step of the viral cycle. **A)** Time-of-addition assay was performed against HCoV-229E in Huh-7/TMPRSS2 cells in the presence of 4 µM HF as previously described in Figure 2A. **B)** Time-of-addition assay was performed against SARS-CoV-2 in Vero-81/TMPRSS2 cells in the presence of 20 µM HF, or 10 µM GC367 and 1 µM Pba, as controls. 10 µM chloroquine was used as a control of TMPRSS2 expression. Cells were lysed 16 h post-infection and lysates subjected to Western blot analysis as previously described. Western blot is representative for 3 independent experiments. **C)** HEK-293TT/ACE2 and Huh-7/TMPRSS2 cells were inoculated with SARSpp and 229Epp, respectively in the presence of increasing concentrations of HF for 2 h. Inoculum was removed and replaced with medium without compound for 46 h. Cells were lysed and luciferase activity was quantified. Data were expressed as mean +/- SEM of 3 independent experiments performed in triplicate. Statistical analyses were performed using the Mann-Whitney nonparametric test. n.s. not significant. * $P < 0.05$, *** $P < 0.001$.

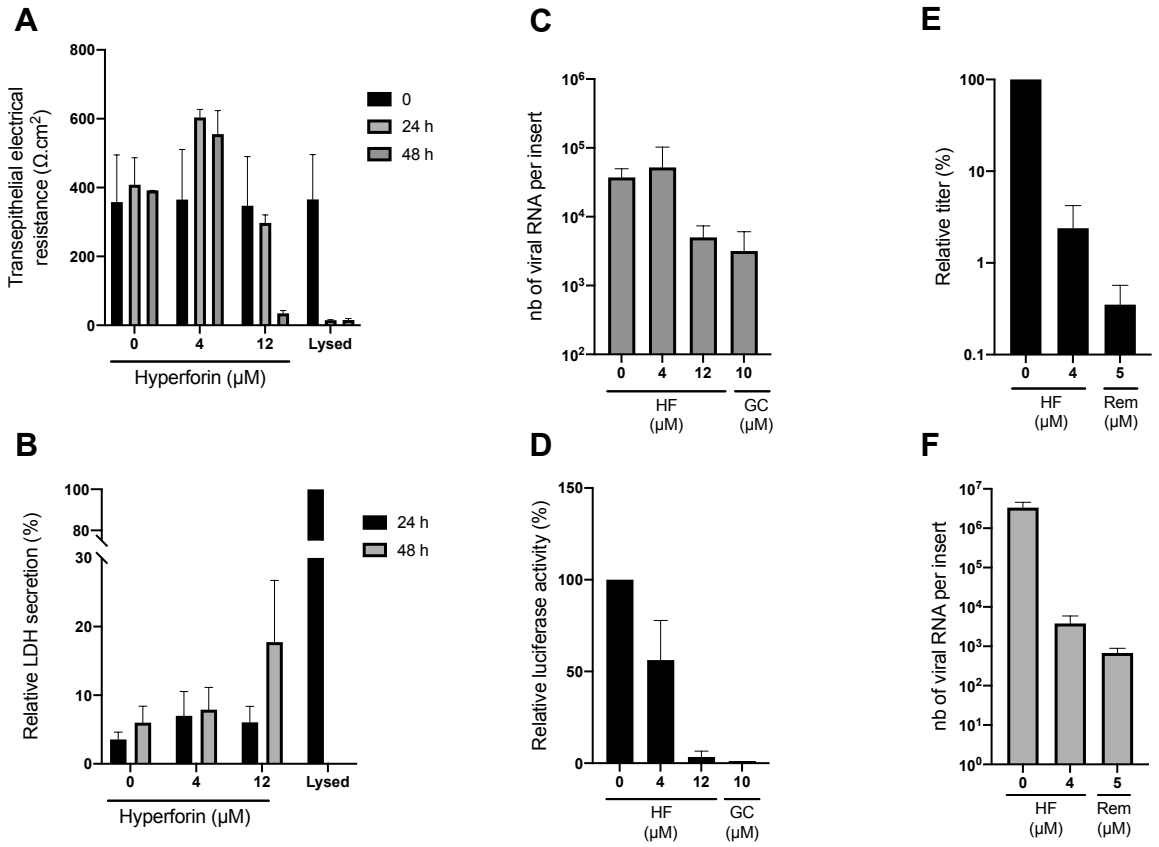

877

878 **Figure 6. HF is active in human primary respiratory epithelial cells.** Cytotoxicity was determined by
879 measuring the TEER (**A**) and LDH secretion (**B**) according to the manufacturer's recommendations. Cells
880 were inoculated with HCoV-229E-Luc at the apical surface of MucilAir™ HAE in the presence of 4 or 12
881 µM HF, and 10 µM GC376 (GC) for 24 h. RNA was extracted from apical wash and was quantified by
882 RT-qPCR (**C**). Cells were lysed and luciferase activity was measured (**D**). Cells were inoculated with
883 SARS-CoV-2 at the apical surface in the presence of 4 µM HF or 5 µM remdesivir (Rem) for 48 h.
884 Infectious virus secreted at the apical surface was quantified by TCID50/mL (**E**) and intracellular viral
885 RNA by RT-qPCR analysis (**F**). Data were expressed as mean +/- SEM of 2 independent experiments.

886

887

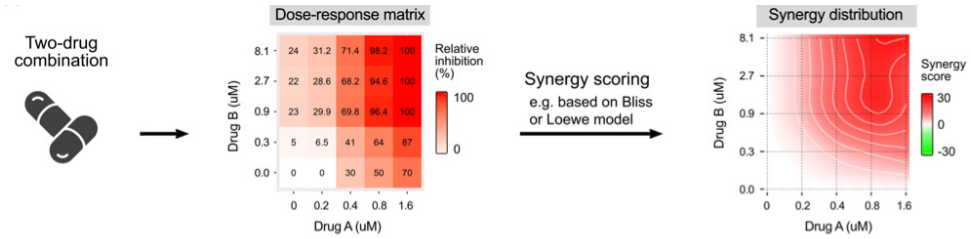

888

889 **Figure 7: Protocol of the combination assay**. Cells (F1G-Red) were treated with increasing
890 concentrations of drug A and drug B and challenged with SARS-CoV-2. The infection was then assessed
891 by confocal microscopy. Nine images per well were taken and infected cell number was quantified.
892 The data were then uploaded on SynergyFinderPlus. Synergy scores were calculated based on 4
893 mathematical models (HSA, Loewe, Bliss and ZIP). The combination is synergistic if the score is above
894 10; additive if it is ranging from -10 to 10; and antagonistic if it is below 10.

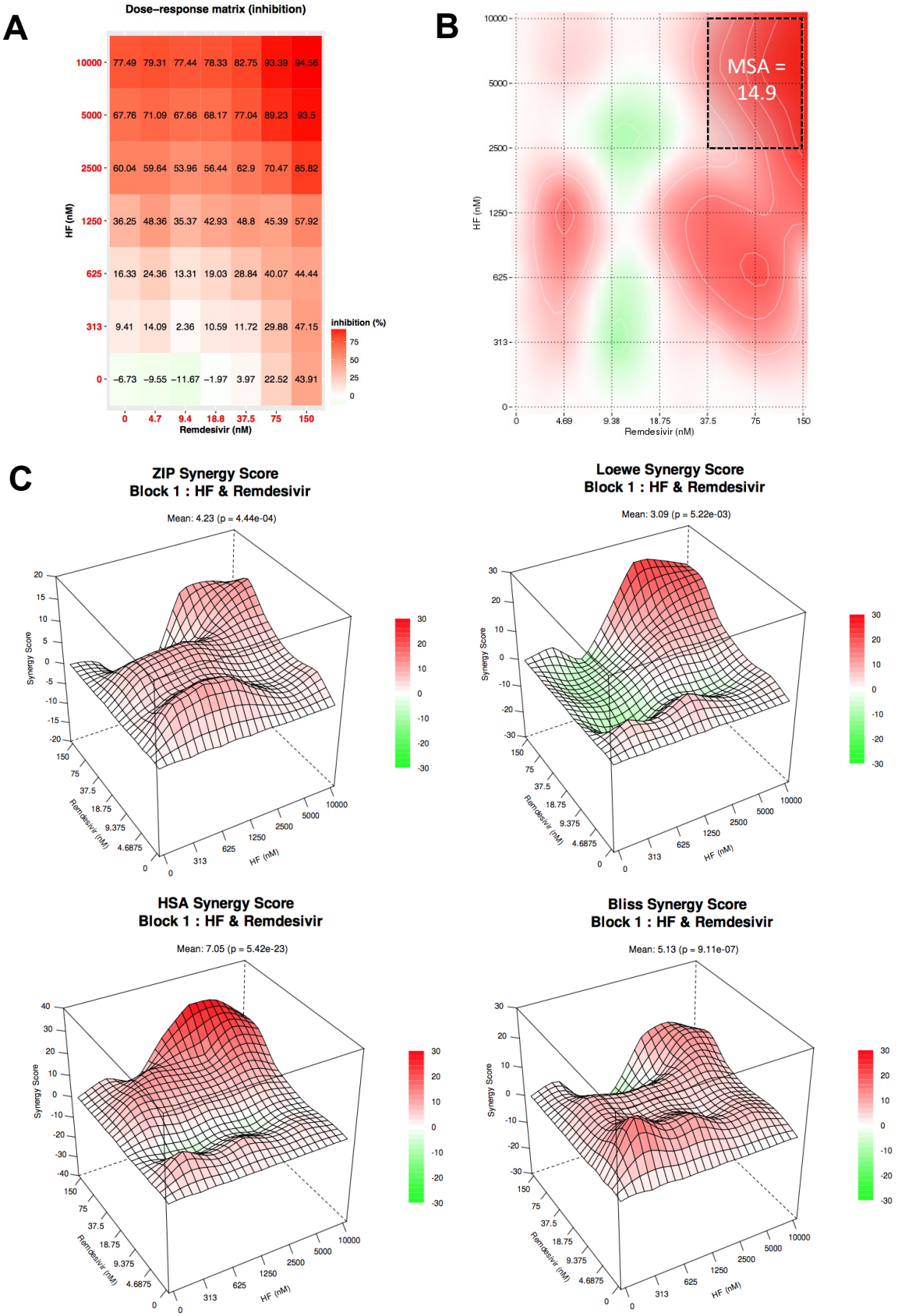

Figure 8. Combination of HF and remdesivir. **A)** Inhibition of infection heatmap. **B)** Most synergistic area (MSA) obtained with SynergyFinder 3.0 for HSA model. **C)** Heatmaps obtained with SynergyFinderPlus.